

# Homoclinic bifurcations leading to the emergence of bursting oscillations in cell models

V.N. Belykh<sup>1</sup>, I.V. Belykh<sup>2</sup>, M. Colding-Jørgensen<sup>3</sup>, and E. Mosekilde<sup>4,a</sup>

<sup>1</sup> Advanced School of General and Applied Physics, Nizhny Novgorod University, 23 Gagarin Ave., Nizhny Novgorod, 603600 Russia

<sup>2</sup> Radiophysical Department, Nizhny Novgorod State University, 23 Gagarin Ave., Nizhny Novgorod 603600, Russia

<sup>3</sup> Scientific Computing, Novo Nordisk A/S, 2880 Bagsværd, Denmark

<sup>4</sup> Center for Chaos and Turbulence Studies, Department of Physics, The Technical University of Denmark, 2800 Lyngby, Denmark

Received 24 June 1999 and Received in final form 17 February 2000

**Abstract.** We present a qualitative analysis of a generic model structure that can simulate the bursting and spiking dynamics of many biological cells. Four different scenarios for the emergence of bursting are described. In this connection a number of theorems are stated concerning the relation between the phase portraits of the fast subsystem and the global behavior of the full model. It is emphasized that the onset of bursting involves the formation of a homoclinic orbit that travels along the route of the bursting oscillations and, hence, cannot be explained in terms of bifurcations in the fast subsystem. In one of the scenarios, the bursting oscillations arise in a homoclinic bifurcation in which the one-dimensional (1D) stable manifold of a saddle point becomes attracting to its whole 2D unstable manifold. This type of homoclinic bifurcation, and the complex behavior that it can produce, have not previously been examined in detail. We derive a 2D flow-defined map for this situation and show how the map transforms a disk-shaped cross-section of the flow into an annulus. Preliminary investigations of the stable dynamics of this map show that it produces an interesting cascade of alternating pitchfork and boundary collision bifurcations.

**PACS.** 05.45.-a Nonlinear dynamics and nonlinear dynamical systems

## 1 Introduction

Living cells depend on the existence of a cell membrane that can maintain an appropriate intracellular environment and regulate the exchanges of ions and molecules between the cell and its surroundings [1]. For many cell types the membrane is excitable, or the membrane potential exhibits complicated patterns of slow and fast oscillations associated with variations of the different ionic currents.

The bursting and spiking dynamics of the membrane potential is essential for the function of the cell as well as for its communication with neighboring cells. It is well known, for instance, that traveling electrical pulses are responsible for the propagation of information along nerve fibers [2]. Fast potassium-controlled oscillations are important for the transmission of signals between nerve and muscle cells and thus for the contractions of the striated muscles [3], and slower, calcium-controlled oscillations are involved in the contractions of smooth muscle fibers [4] as well as in the function of rhythmogenic nerves [5]. It

has also been demonstrated that the excretion of insulin from pancreatic  $\beta$ -cells depends on the fraction of time that the cells within an islet of Langerhans spend in the spiking state. This fraction again varies with the concentration of glucose in the extracellular liquid [6,7]. It is obviously of interest to understand these phenomena in detail, and over the years significant effort has been devoted to studying the ionic transport mechanisms of the cell membrane.

With the introduction of patch clamping techniques [8] it has become possible to measure the ionic currents through the various channels as a function of the membrane potential and in dependence on the concentrations of ions and molecules. This has led to the formulation of a variety of mathematical models describing the most important physiological processes for different cell types [9–16]. Despite this effort, the biological mechanisms underlying the bursting behavior are not yet fully understood. For pancreatic  $\beta$ -cells, for instance, it is not known in what way calcium is involved in the slow dynamics [15]. It also appears that regular bursting behavior only arises in clusters of closely coupled  $\beta$ -cells. For isolated cells, stochastic

---

<sup>a</sup> e-mail: ellen@chaos.fys.dtu.dk

effects associated with the opening and closing of potassium channels tend to produce irregular spiking [17].

At the same time, a number of phenomenological models have been proposed [18]. Without direct relation to concrete physiological mechanisms, such models aim at reproducing the characteristic features of the bursting behavior. To the extent that the assumptions underlying the phenomenological models are sufficiently general, these models may be used to explain generic bifurcation scenarios that can also be observed in the more realistic models.

The purpose of the present investigation is to perform a more rigorous analysis of the mechanisms leading to the onset of bursting. Recent studies [19–21] suggest that there are a significant number of unresolved problems in this area, particularly concerning the emergence of very complicated dynamics in the transitions between bursting and continuous spiking and between different bursting states [22, 23]. It is important to eliminate the widespread misconception that the onset of bursting can be explained in terms of bifurcations that occur in the fast subsystem. Bursting emerges as a result of the creation of a homoclinic orbit traveling along the route of the bursting oscillations in the full system. The difficulty of the analysis is connected with the fact that the smaller the parameter  $\mu$  describing the rate of change of the slow system is, the finer the bifurcational structure of the model, and the harder the computational problem will be.

Considering the Hindmarsh-Rose system and similar classes of cell models, Wang [19] has proposed the combination of two different mechanisms to explain the genesis of bursting. First, the continuously spiking state undergoes a period-doubling transition to a state of chaotic firing, and this state is destabilized in a boundary crisis. Bursting then arises through the realization of a homoclinic connection that serves as a reinjection mechanism for the chaotic saddle. In this picture the bursting oscillations are described as a form of intermittency with the silent state corresponding to the normal turbulent phase and the firing state to the laminar phase. Wang supports his analysis by a calculation of the escape rate from the chaotic saddle and outlines a symbolic dynamics formalism to characterize the various bursting states. Wang's discussion is compelling in many ways and it agrees with numerically obtained bifurcation diagrams, Poincaré sections and return maps. However, the essential question as to how the homoclinic connection arises is left unanswered.

Terman [20, 21] has performed a more complete and detailed analysis of the onset of bursting oscillations. He has obtained a two-dimensional (2D) flow-defined map for the most complex scenario where the equilibrium point of the full system falls close to a saddle point of the fast subsystem, which has a homoclinic orbit. By means of this map, Terman has proved the existence of a hyperbolic structure (a chaotic saddle) similar in many respects to a Smale horseshoe. This represents an essential step forward in understanding the complexity involved in the emergence of bursting. However, since Terman's set is non-attracting, it cannot be related directly to the observed stable bursting phenomena. The reason for this result is that Terman in

his analysis of the flow-defined map restrains himself to consider only half of the map and concentrates his analysis on the effects of rotations caused by the dynamics of the fast subsystem. Neglecting as a first approach these rotations we shall derive an explicit representation of the full 2D map both for the symmetric and the asymmetric case, and we shall prove that the map can produce an attracting chaotic state.

Our analysis proceeds along the following scheme: The basic model and the corresponding assumptions are presented in Section 2. We consider a generic cell model in the form of a 3D system of differential equations with two fast and one slow variable. Section 3 presents a set of theorems on invariant manifolds, cycles and simple homoclinic orbits in generic systems of differential equations with a single slow variable and discusses the relation between the global dynamics of the full system and the phase portrait of the fast subsystem. Based on these theorems, Section 4 presents four different scenarios for the onset of bursting in our generic cell model. Although these scenarios may appear similar to the scenarios described in the more conventional analysis in which the model is decomposed into a fast and a slow subsystem, we emphasize that each of the transitions represents a bifurcation of the full 3D system and is essentially different from the bifurcations of the fast subsystem.

In the most interesting scenario, the emergence of bursting oscillations is associated with a homoclinic bifurcation in which the 1D stable manifold of a saddle point becomes attracting to its whole 2D unstable manifold. This type of homoclinic bifurcation does not appear to have been examined in detail. In Section 5 we derive a flow-defined map appropriate for this situation and demonstrate how the map transforms a disk transverse to the flow into an annulus. In Sections 6 and 7 explicit forms for this two-dimensional map are obtained for the symmetrical and asymmetrical cases. In good agreement with our qualitative analysis of the cell model, the bifurcation diagrams of these maps display complicated sets of bifurcations in the transition to chaotic bursting.

Considering the various codimension-1 bifurcations that can occur in the fast subsystem, Hoppensteadt and Izhikevich [24] have established a complete classification of the so-called planar point-cycle fast-slow codimension-1 bursters. The term point-cycle here refers to the case where the silent state is an equilibrium point and the spiking state a limit cycle. When the silent state is a small amplitude limit cycle, the burster is said to be of cycle-cycle type. The word planar refers to the case when the fast subsystem is two-dimensional. Although we shall refer to the Hoppensteadt-Izhikevich classification in connection with the four scenarios presented in Section 4, we emphasize that the onset of bursting takes place via a homoclinic bifurcation in the full system and not via a codimension-1 bifurcation in the fast subsystem. Hence, our four mechanisms for the onset of bursting are not directly related to the above classification.

## 2 The cell model

Models of oscillating and bursting biological cells can often be cast into the general form [11–13]

$$\begin{cases} \dot{x} = P(x, y, z), \\ \dot{y} = Q(x, y), \\ \dot{z} = \mu(R(x, y) - z), \end{cases} \quad (2.1)$$

where  $\mu$  is a small positive parameter, and where the continuous functions  $P(x, y, z)$ ,  $Q(x, y)$ , and  $R(x, y)$  have the following properties:

1) The partial derivatives of  $P$ ,  $Q$ , and  $R$  are sufficiently smooth. In order to use bifurcation theory we need at least  $P, Q, R \in \mathbb{C}^3$  for  $(x, y, z) \in \mathbb{R}^3$  (or  $(x, y, z) \in G \subset \mathbb{R}^3$ ).

2) The system of equilibrium conditions  $Q(x, y) = 0$ ,  $R(x, y) = z$  defines a function

$$z = R(x, y = q(x)) \equiv g(x). \quad (2.2)$$

3) The equilibrium conditions  $P(x, y, z) = 0$ ,  $Q(x, y) = 0$  determine a branch of solutions with respect to  $z$  such that

$$z = p(x, y = q(x)) \equiv f(x). \quad (2.3)$$

Under these conditions, the equilibrium points of (2.1) are given by the points of intersection of the functions (2.2) and (2.3). The curve  $z = f(x)$  determines the equilibria of the  $z$ -parameter family of fast two-dimensional systems

$$\dot{x} = P(x, y, z), \quad \dot{y} = Q(x, y), \quad z = \text{const}, \quad (2.4)$$

obtained from (2.1) for  $\mu = 0$  and, through its crossing points with the curve  $z = f(x)$ , the function  $z = g(x)$  determines the equilibria of the full system for  $\mu > 0$ .

In the following analysis we assume that the function  $f(x)$  has two critical points  $x_1^c$  and  $x_2^c$  such that

$$\begin{aligned} f' &> 0, & x_1^c < x < x_2^c, \\ f' &< 0, & x < x_1^c, \quad x > x_2^c, \end{aligned} \quad (2.5)$$

and that the curve  $g(x)$  intersects  $f(x)$  in a single point  $x_e$ . Within the region of interest, the cell model (2.1) then displays a unique equilibrium point  $E(x_e, y_e, z_e)$ , where  $z_e = f(x_e) = g(x_e)$  and  $y_e = q(x_e)$ . At least in an interval around the equilibrium point, we require that  $g$  has a larger slope than  $f$ .

We finally assume that the divergence of the two-dimensional vector field  $\mathcal{F}(P, Q)$  changes sign so that

$$\begin{aligned} \sigma(x) &\equiv \text{div} \mathcal{F}|_{z=f(x)} > 0, & x_{H1} > x > x_{H2}, \\ \sigma(x) &< 0, & x < x_{H1}, \quad x > x_{H2}, \end{aligned} \quad (2.6)$$

where the values  $x_{H1,2}$  correspond to a pair of Hopf bifurcations of the equilibrium point for the fast system (2.4). The Hopf bifurcations may be sub- or supercritical, and one or both of the bifurcations may fall outside the region of interest  $(x, y, z) \in G$ . In the case of a subcritical Hopf

bifurcation at  $x_{H1}$ , the generated unstable limit cycle is assumed to stabilize in a saddle-node bifurcation at  $x_{+1}$ .

A simple example of a model that satisfies the above conditions is the well-known Hindmarsh-Rose system [18]. However, these conditions are also in accordance with typical biophysical models such as, for instance, the three-variable Chay-Kaiser model [11]. The conventional analysis of this type of model [12] applies a decomposition of the full system into a two-dimensional fast subsystem described by equation (2.4) and a slow system accounting for the variation of  $z$ . In relation to the fast dynamics,  $z$  is then considered as a parameter that shifts the working point forth and back. This approach is obviously inadequate, however, since it fails to account for some of the most interesting aspects of the models, namely the appearance of chaotic dynamics. Moreover, the onset of bursting oscillations involves the formation of a homoclinic connection in the full model and, hence, cannot be explained in terms of bifurcations that occur in the fast subsystem.

## 3 Manifolds and cycles for generalized cell models

Consider the general system

$$\begin{aligned} \dot{x} &= X(x, z) + \mu V(x, z, \mu), \\ \dot{y} &= \mu Z(x, z, \mu), \end{aligned} \quad (3.1)$$

where  $x \in \mathbb{R}^n$  describes the dynamics of an  $n$ -dimensional fast subsystem, and  $z \in \mathbb{R}^1$  is a single slowly varying coordinate.  $X$ ,  $V$  and  $Z$  are assumed to be sufficiently smooth vector, respectively, scalar functions, and  $\mu > 0$  is a small parameter. Let us start by introducing some theorems concerning the behavior of systems of the form (3.1), derived originally by Belykh [25], in order to apply them to our generic cell model (2.1).

For all  $z \in \mathbb{R}^1$  the reduced system

$$\dot{x} = X(x, z), \quad z = \text{const} \quad (3.2)$$

is assumed to have a set of equilibrium states  $x = x_k(z)$  with  $X(x_k, z) = 0$ ,  $k = 0, 1, 2, \dots$

**Theorem 1.** 1) *Let the eigenvalues of the Jacobian matrix  $X_x(x_k(z), z)$  be separated from the imaginary axis for  $z \in \mathbb{R}^1$ . Then there exists a number  $\mu_0 > 0$  such that if  $\mu \in (0, \mu_0)$ , (3.1) has a unique one-dimensional integral manifold  $J_k(\mu) = \{x = \tilde{x}_k(z, \mu), z \in \mathbb{R}^1\}$  close to the reduced manifold  $J_k(0) = \{x = x_k(z)\}$  and with  $\tilde{x}_k(z, 0) = x_k(z)$ .*

2) *If the eigenvalues of  $X_x(x_k(z), z)$  are to the left (right) of the imaginary axis then the manifold  $J(\mu) \equiv J_k(\mu)$  is stable (unstable, respectively).*

3) *If  $m$  eigenvalues are to the left and  $n - m$  eigenvalues to the right of the imaginary axis then the manifold  $J(\mu)$  is of saddle type, and given by the intersection of the corresponding stable and unstable manifolds,  $J(\mu) \in W^s(\mu) \cap W^u(\mu)$ . Being continuous in the parameter  $\mu$ , the manifolds  $W^{s(u)}(\mu)$  are close to the reduced*

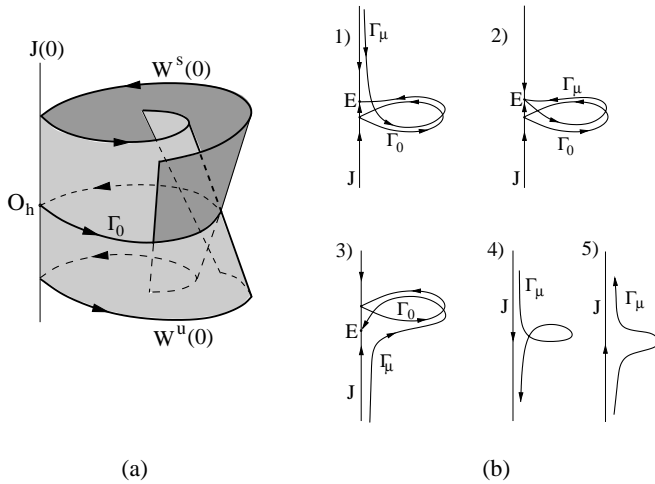


**Fig. 1.** (a) Conditions of Theorem 2. . The stable and unstable manifolds of the saddle branch  $J(0)$  for the fast subsystem intersect along the homoclinic orbit  $\Gamma_0$ . (b) Different forms of homoclinic orbits  $\Gamma_\mu$  to the saddle manifold  $J(\mu)$  for the full cell model, depending on the mutual arrangement of the equilibrium point  $E$  and the homoclinic orbit  $\Gamma_0$ . In case (2), the equilibrium point has a homoclinic orbit  $\Gamma_\mu$  close to the homoclinic loop of the saddle point  $O_h$ .

manifolds  $W^{s(u)}(0)$ . This closeness is maintained outside of a small neighborhood of  $J(\mu)$  for pieces of  $W^{s(u)}(\mu)$  corresponding to the finite time continuation by the flow.

4) The motion on  $J_k(\mu)$  is defined by the first-order equation

$$\dot{z} = \mu Z(x_k(z, \mu), z, \mu). \quad (3.3)$$

**Theorem 2.** 1) Let the saddle-type equilibrium point  $O_h = \{x_0(z), z = z_0\}$  of the reduced system (3.2) have a homoclinic orbit  $\Gamma_0$  which is the transversal intersection of the manifolds  $W^s(0)$  and  $W^u(0)$  :

$$\dim(W_M^s \cap W_M^u) = 1, \quad (3.4)$$

where  $W_M^{s(u)}$  are the tangent manifolds to  $W^{s(u)}(0)$  at the point  $M \in \Gamma_0$ . The system (3.1) then has the homoclinic (doubly asymptotic) orbit  $\Gamma_\mu$  to the manifold  $J(\mu)$ .

2) If the point  $O_h = \{x_0(z), z = z_0\}$  is an equilibrium point of (3.1) then the saddle  $\tilde{O}_h$  existing after a perturbation of (3.1) has the homoclinic orbit  $\Gamma_\mu$ .

Figure 1(a) illustrates the conditions of Theorem 2. , and figure 1(b) shows different types of homoclinic orbits to  $J(\mu)(= J)$  depending on the mutual arrangement of the equilibrium point  $E$  of (3.1) and the homoclinic loop  $\Gamma_0$  of (3.2). In situation 2),  $\Gamma_\mu$  is a homoclinic orbit to the equilibrium point  $E$ , and  $\Gamma_0$  is a homoclinic orbit to the nearby saddle point  $O_h$ . Note that in the cases where (3.1) has no equilibrium for  $Z(x, z, \mu) > 0 (< 0)$ , the one-dimensional manifold  $J(\mu)$  is a trajectory of (3.1), and  $\Gamma_\mu$  is a homoclinic orbit for it. For example, if (3.1) is periodic in  $z$  and  $Z > 0$ , then  $J(\mu)$  is a periodic orbit, and the neighborhood of  $\Gamma_\mu$  has a complex set of trajectories.

Let the reduced system (3.2) for all  $z \in \mathbb{R}^1$  have a limit cycle  $L_0 = \{x = \zeta_0(t, z)\}$  of period  $\tau(z) = 2\pi/\omega(z)$ . For simplicity we consider the 3-dimensional case of (3.1) for which the vector  $x$  represents  $(x, y) \in \mathbb{R}^2$ . Thus we denote  $L_0 = \{x = \zeta_0(t, z), y = \eta_0(t, z)\} \in \mathbb{R}^2$ ,  $\zeta_0 = (\zeta_0, \eta_0)$ , and  $X = (P(x, y, z), Q(x, y, z))$  in (3.1). In accordance with Belyustina and Belykh [26] we get the following assertion:

**Theorem 3.** Assume that for all  $z \in \mathbb{R}^1$  the characteristic exponents of  $L_0$

$$h = \frac{1}{\tau(z)} \int_0^{\tau(z)} \operatorname{div} X(\zeta_0(t, z)) dt \neq 0. \quad (3.5)$$

Then for  $\mu \in (0, \mu_0)$  the system (3.1) has a cylindrical manifold  $L_\mu = \{x = \zeta(\varphi, z, \mu), z \in \mathbb{R}^1\}$  stable for  $h < 0$  and unstable for  $h > 0$ . The differential equation for  $L_\mu$  can be written in the form

$$\begin{cases} \dot{\varphi} = \omega(z) + r(\varphi, z, \mu), \\ \dot{z} = \mu Z(\zeta(\varphi, z, \mu), z, \mu), \end{cases} \quad (3.6)$$

where  $\zeta(\varphi, z, \mu) \rightarrow \zeta_0(\varphi, z)$  and  $r(\varphi, z, \mu) \rightarrow 0$  for  $\mu \rightarrow 0$  are both  $2\pi$ -periodic in  $\varphi$ .

Note that the manifolds  $J(\mu)$  and  $L_\mu$  defined in these theorems are unbounded in  $z$ . Hence, the theorems cannot be applied directly to models like (2.1), where the manifolds of the reduced system have edges. In order to match Theorems 1. -3. to system (2.1) we use the following standard “freezing” procedure. Instead of system (3.1) we consider a system  $(3.1)_0$  coinciding with (3.1) in the interval  $(z_1, z_2)$  and extended beyond this interval by  $X(x, z) = X(x, z_1)$  for  $z \leq z_1$  and  $X(x, z) = X(x, z_2)$  for  $z \geq z_2$ . If the conditions of Theorems 1. -3. hold for system (3.1) in the interval  $(z_1, z_2)$ , then these conditions hold for system  $(3.1)_0$  for  $\forall z \in \mathbb{R}^1$ . Hence, if system  $(3.1)_0$  has the manifolds  $J(\mu)$  and  $L_\mu$  then those parts of these manifolds that fall in the interval  $(z_1, z_2)$  serve as integral manifolds of system (3.1). In the following we shall assume that such a procedure is used as we return to the cell model (2.1).

Excluding two regions  $T_{1,2}$  around the critical points of the function  $z = f(x) : T_{1,2} = \{|f(x_{1,2}^c) - z| < \varepsilon(\mu)\}$ , where  $\varepsilon(\mu) > 0$  is small, we can distinguish three branches of the equilibrium point curve in  $\mathbb{R}^3$  defined by equation (2.3). We denote the left, middle, and right branches of the equilibrium curve of the fast system by  $J_1(0)$ ,  $J_0(0)$ , and  $J_2(0)$ , respectively.

Theorem 1. can immediately be applied to the manifolds  $J_1(0)$  and  $J_0(0)$ . This implies that for  $\mu > 0$  there exists a stable manifold  $J_1(\mu)$  in the region  $\{z > f(x_1^c) + \varepsilon, x < x_1^c\}$ , and in the region  $\{f(x_1^c) + \varepsilon < z < f(x_2^c) - \varepsilon, x_1^c < x < x_2^c\}$  there exists a saddle manifold  $J(\mu) = J_0(\mu)$  arising as an intersection of stable  $W^s$  and unstable  $W^u$  manifolds. For  $J_2(0)$ , Theorem 1. does not apply because the equilibrium point undergoes a Hopf bifurcation, and the theorem related to the so-called slow passage effect has to be used [27] .

Obviously, if the surface  $z = R(x, y)$  ( $\dot{z} = 0$ ) intersects the above manifolds in points outside  $T_{1,2}$ , the regions  $T_{1,2}$  can be considered as transition layers for the flow in the neighborhood of  $J_k(\mu)$ , and the trajectories (including  $J(\mu)$ ) pass these transition layers during times of the order of  $2\varepsilon(\mu)/\mu$ . On the other hand, if  $O = (\{z = R(x, y)\} \cap J_k(\mu)) \in T_{1,2}$ , then the intersection point  $O$  is at the edge of  $J_k$ , and specific phenomena may occur.

Now we exclude four additional transition regions  $T_S = \{|z_S - z| < \varepsilon(\mu)\}$ , where the subscript  $S = H1, H2, +1$ , and  $h$ , and the values  $z_S$  refer to the fast system Hopf, saddle-node on a cycle, and homoclinic orbit bifurcations, respectively. Again,  $\varepsilon(\mu) > 0$  is assumed to be small. Outside  $T_S$ , Theorem 3. can be applied for the cylindrical manifolds  $L_\mu^s$  and  $L_\mu^u$  that have appeared from the reduced manifolds formed by the  $z$ -family of stable, respectively, unstable cycles of system (2.1) in the cases described as scenarios 2 and 4 in Section 4. The differential equations (3.6) for  $L_\mu^s$  (or  $L_\mu^u$ ) can be rewritten in the form

$$\begin{cases} \dot{\varphi} = \omega(z) + r(\varphi, z, \mu), \\ \dot{z} = \mu(R(\xi(\varphi, z), \eta(\varphi, z)) - z) + \mu\tilde{r}(\varphi, z, \mu), \end{cases} \quad (3.7)$$

where the functions  $r(\varphi, z, \mu)$  and  $\tilde{r}(\varphi, z, \mu)$  both vanish at  $\mu = 0$ .

**Theorem 4.** *Given the integral*

$$I(z) = \frac{1}{\tau(z)} \int_0^{\tau(z)} (R(\zeta_0(t, z)) - z) dt, \quad (3.8)$$

1) if  $I(z) \neq 0$  then the manifold  $L_\mu$  is transient for the flow (2.1). Namely, for  $I(z) < 0$  ( $> 0$ ) all trajectories in  $L_\mu$  are rotating in  $\varphi$  and increasing (decreasing, respectively) in  $z$ .

2) if  $I(z)$  changes sign then the system (2.1) has a limit cycle  $L_\mu^0 \in L_\mu$ . This cycle is unique and stable (unstable) in  $L_\mu$  if  $I'(z_0) < 0$  ( $> 0$ , respectively) for  $I(z_0) = 0$ .

**Proof.** The system at the cylinder (3.7) can be transformed into the form of a single first-order differential equation

$$\frac{dz}{d\varphi} = \mu \frac{R(\zeta_0(\varphi, z)) - z}{\omega(z)} + \mu r_0(\varphi, z, \mu), \quad (3.9)$$

where  $\lim_{\mu \rightarrow 0} r_0 = 0$ . Applying the usual averaging method, originally developed by Pontrjagin [28], instead of (3.9) we obtain an equation written in terms of the time variable

$$\frac{dz}{dt} = \mu I(z). \quad (3.10)$$

Then transitivity follows from  $dz/d\varphi \neq 0$  for  $I(z) \neq 0$ , and zeros of  $I(z)$  define the limit cycles for which the stability is determined by the derivative  $I'(z)$ .  $\square$

For the unstable manifold  $L_\mu^u$  we obtain similar results except that in this case we have a saddle-type or a strongly unstable cycle.

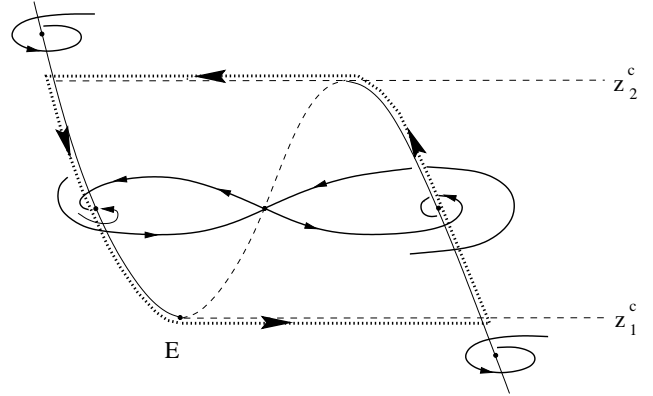


**Fig. 2.** Formation of a homoclinic orbit in the full cell model according to scenario 1. The family of phase portraits of the fast subsystem is shown as a parameter- $z$  bifurcation diagram. The dotted curve illustrates the route for the bursting oscillations. We have argued for the emergence of these oscillations via a codimension-2 saddle-node bifurcation in the full cell model.

**Statement.** Let the surface  $z = R(x, y)$  intersect the curve  $z = f(x)$  defined by (2.3) in the point  $z = z_h$  for which the reduced system saddle  $O_h$  has a homoclinic orbit. Then, due to Theorem 2., a saddle point  $\hat{O}_h$  of the system (2.1) with a function  $R(x, y) + c(\mu)$  replacing  $R(x, y)$  has a homoclinic orbit. Here,  $c(\mu)$  is a constant (independent of  $x$  and  $y$ ) that vanishes for  $\mu = 0$ .

## 4 Bifurcation scenarios for bursting oscillations

Based on the above analysis we can present four different scenarios for the emergence of bursting oscillations in the generic cell model (2.1):

**Scenario 1.** Recall first our assumption of a unique equilibrium point  $E(x_e, y_e, z_e)$ , where  $x_e$  is determined by the intersection  $f(x_e) = g(x_e)$ ,  $y_e = q(x_e)$ , and  $z_e = f(x_e)$ . If  $x_e = x_1^c$ , the simple picture of Figure 2 is realized. Consider  $l = x_e - x_1^c$  as a bifurcation parameter. For  $l = 0$ ,  $E$  is a saddle-node (with two vanishing eigenvalues) and the equilibrium point has a homoclinic orbit traveling along the route: 1D unstable manifold of  $E \rightarrow T_1 \rightarrow U(J_2(\mu)) \rightarrow T_2 \rightarrow U(J_1(\mu)) \rightarrow E$ . Here,  $U(J_k(\mu))$  denotes a small neighborhood of the manifold  $J_k(\mu)$ . For  $l < 0$ ,  $E$  is stable and attracts the whole phase space, and for  $l > 0$ ,  $E$  becomes a saddle point. A stable limit cycle is then generated from the homoclinic orbit that was born at the bifurcation point (for an overview of the bifurcation scheme see Fig. 8(a), below). It is important to realize the difference between this transition and the normal bifurcation for the birth of a limit cycle via a saddle-node bifurcation. The basin of the cycle is the whole 3D phase space except for the saddle point  $E$  and its 1D stable manifold. The route of the bursting oscillations is indicated by the dotted curve in Figure 2.

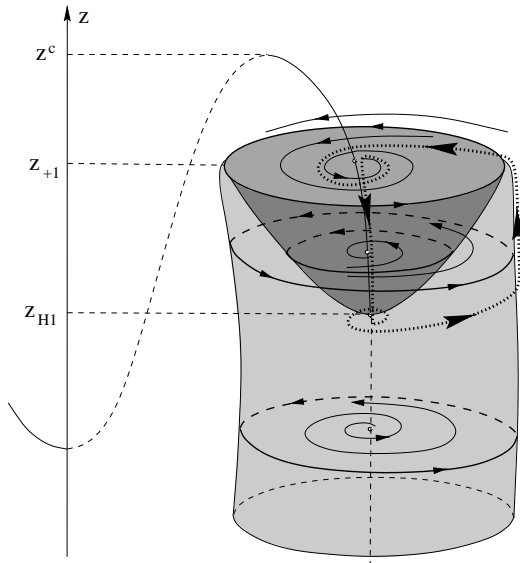


**Fig. 3.** Emergence of bursting oscillations in the full cell model following scenario 2. The family of phase portraits of the fast subsystem is shown as a parameter- $z$  bifurcation diagram. The dotted curve illustrates the route of the bursting oscillations.

The above codimension-2 bifurcation also differs from the usual bifurcation of a saddle-node with a homoclinic orbit where a cycle is generated simultaneously with the disappearance of two equilibrium points. In cases when the condition that the slope of  $g$  is larger than the slope of  $f$  does not hold, and the system (2.1) has two nearby equilibrium points, one may observe all the peculiarities of a Bogdanov-Takens bifurcation [27], including Hopf and local homoclinic loop bifurcations. The transition  $T_1 \rightarrow U(J_2(\mu))$  with the isolated small limit cycle observed in the Chay model [23] may be explained by this mechanism.

Finally we note that it does not matter for the present scenario which type of attractor is located along the right branch of curve  $z = f(x)$ . The stable manifold  $L_\mu^s$  may stand for  $J_2(\mu)$ . Hence, in relation to the classification of point-cycle bursters introduced by Hoppensteadt and Izhikevich [24] this scenario describes the mechanism involved in the formation of so-called fold/circle, circle/circle, Hopf/circle, subHopf/circle, fold/Hopf, circle/Hopf, Hopf/Hopf, and subHopf/Hopf bursters.

**Scenario 2.** Let the conditions of Figure 3 be realized and let the bifurcation parameter be  $l = z_{H1} - z_e$ . For  $l < 0$ ,  $E$  is a stable focus, and the edge of its two-dimensional focus submanifold is a saddle-type cycle  $C^{sd}$  existing according to Theorem 4. The basin of attraction for  $E$  is the whole phase space excluding  $C^{sd}$  and its cylindrical stable manifold. For  $l = 0$ , a homoclinic orbit bifurcation, being simultaneously a subcritical Hopf bifurcation, occurs. For  $l > 0$ , bursting oscillations explosively arise and travel the route:  $T_{H1} \rightarrow U(L_\mu^s) \rightarrow T_{+1} \rightarrow U(J_2(\mu)) \rightarrow T_{H1}$ , if the integral  $I(z)$  is positive for  $L_0^s$  (see dotted curve in Fig. 3). As previously indicated, the tran-

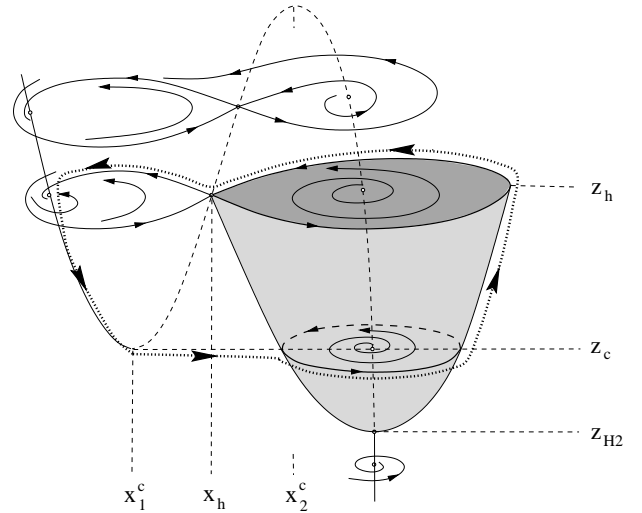


**Fig. 4.** Family of phase portraits shown as a parameter- $z$  bifurcation diagram for the conditions of scenario 3. The fast subsystem displays a supercritical Hopf bifurcation at  $z_{H2} < z_c$  and a homoclinic loop bifurcation at  $z_h > z_c$ . The dotted curve illustrates the route for the bursting oscillations in the full system.

sition  $U(J_2(\mu)) \rightarrow U(L_\mu^s)$  through the layer  $T_{H1}$  occurs with the delayed loss of stability [27]. The general scheme for such a transition, leading to so-called elliptic bursting [29], will be presented in Figure 8(b). Note that in order to satisfy the condition  $I(z) > 0$ , the larger part of  $L_0^s$  must be in the region  $z > R(x, y)$  of phase space. We omit the details of this analysis referring to the complicated bifurcation sets described by Belyakov [30] and Arnold *et al.* [27]. We emphasize only the following important feature: The bifurcation leading to the emergence of bursting is not the Hopf bifurcation of the fast subsystem but the formation of a homoclinic orbit traveling along the route of bursting. A similar scenario was described in 1980 by Belykh and Chertkov [31] for the Hodgkin-Huxley model.

**Scenario 3.** Here we assume that the conditions corresponding to Figure 4 are realized and take the bifurcation parameter  $l = z_e - z_h$ , with  $z_h$  representing the point of homoclinic bifurcation for the fast subsystem. In the Hoppensteadt-Izhikevich classification [24], this scenario describes the mechanism of formation of the so-called fold/homoclinic, circle/homoclinic, Hopf/homoclinic, and subHopf/homoclinic bursters. Note, however, that in this classification the term homoclinic refers to a homoclinic bifurcation in the fast subsystem.

It follows from results on system behavior in the transition regions (see Terman [21]) that for each small negative  $l < 0$  there exists a value of  $\mu_b(l)$  such that for  $\mu \in (0, \mu_b(l))$  the system (2.3) has a bursting oscillation. The route of this bursting is  $T_h \rightarrow U(J_1(\mu)) \rightarrow T_1 \rightarrow U(L_\mu^s) \rightarrow T_h$ . We denote the inverse function to  $\mu_b(l)$  by  $l = l_b(\mu)$ . For any small positive parameter  $l > 0$ , the separating surface  $\{R(x, y) - z = 0\}$  cuts a small piece of the homoclinic orbit for the fast system close to the

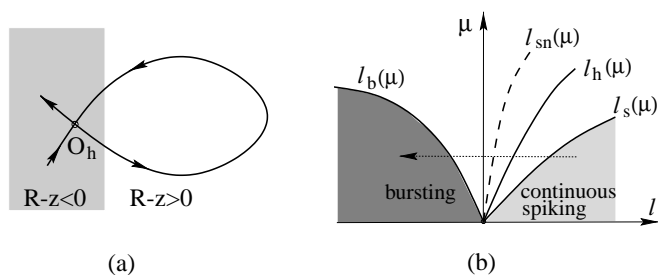


**Fig. 5.** (a) For  $l = z_e - z_h > 0$ , part of the homoclinic loop for the fast subsystem falls in the region where the contribution to the integral  $I(z_h)$  is negative. (b) Basic bifurcation diagram for the transition from continuous spiking to bursting (as the parameter  $l = z_e - z_h$  is reduced).  $\mu \neq 0$  but small is the parameter that characterizes the slow time scale.  $l_h(\mu)$  is a curve of homoclinic bifurcations for the full system, and  $l_{sn}(\mu)$  is a curve of saddle-node on cycle bifurcations.

saddle  $O_h$  (see Fig. 5(a)). The value of  $(R(x, y) - z)$  is negative for this piece. Hence, the limit of the integral  $I(z_h)$  in (3.8), corresponding to integration along the homoclinic loop  $(x, y) = \zeta_0(t, z_h)$ , becomes negative because  $\lim_{z \rightarrow z_h} \tau(z) = \infty$  and the larger part of the period  $\tau(z)$  for small  $l > 0$  falls at the vicinity of  $O_h$  with negative value of  $(R - z)$ . On the other hand, for the values  $z$  somewhat less than  $z_h$ , the integral  $I(z)$  is positive. Hence, for any small  $l > 0$  there exists a value  $\mu_s(l)$  such that for  $\mu \in (0, \mu_s(l))$  the system (2.1) has a stable limit cycle at  $L_\mu$  corresponding to continuous spiking. Here,  $\mu_s(l)$  denotes the inverse function of  $l = l(\mu_s)$ . We observe that the integral  $I(z_h)$  is similar to Mel'nikov's function.

From Theorem 2. it follows that the system (2.1) has a homoclinic orbit of  $E$  for  $l = l_h(\mu)$ . As illustrated in Figure 5(b),

$$l_b(\mu) < l_h(\mu) < l_s(\mu), \quad (4.1)$$

and as a first result we conclude that a homoclinic orbit bifurcation occurs at the transition from continuous spiking to bursting oscillations for  $\mu = \text{const} > 0$ .

Now we note that the saddle  $O_h$  of the fast subsystem has a negative saddle number  $\sigma = -\lambda + \gamma < 0$ , where  $-\lambda$  and  $\gamma$  are eigenvalues of the linearized fast system at  $O_h$ . This (and only this) property allows a stable limit cycle to link to a homoclinic loop. For any  $\mu > 0$  and for the assumed disposition of the curves  $z = f(x)$  and  $z = g(x)$ , the saddle  $E|_{l=0} = O_h$  of system (2.1) acquires a positive eigenvalue  $\mu^+ = k\mu + o(\mu^2) > 0$  in addition to the eigenvalues  $-\lambda + o(\mu)$  and  $\gamma + o(\mu)$ . This eigenvalue corresponds to an instability of  $E$  along the 1D saddle manifold  $J_0(\mu)$ .

As  $\mu^+$  is the smaller of the positive eigenvalues  $(\mu^+, \gamma + o(\mu))$ , and  $|-\lambda + o(\mu)| > \mu^+$ ,  $\mu^+$  defines the leading direction such that a saddle cycle with 2D stable and 2D unstable manifolds is generated from the homoclinic loop [32] when  $l$  moves away from  $l_h(\mu)$ . In case of the opposite relation between the slopes of the separating surface  $\{R - z = 0\}$  and the equilibrium curve  $z = f(x)$  (*i.e.*, if  $f$  has a larger slope than  $g$ )  $E$  becomes

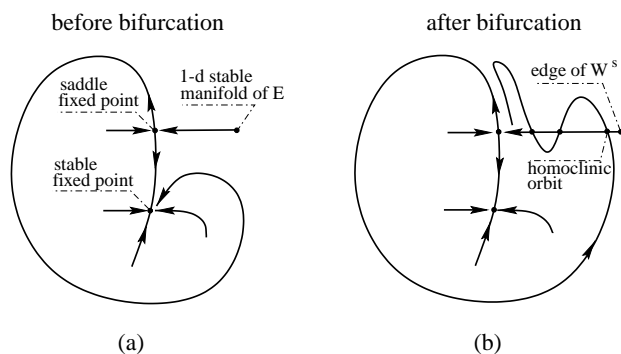


**Fig. 6.** Poincaré section to illustrate the homoclinic orbit bifurcation of a saddle cycle (curve  $l_h(\mu)$  in Fig. 5) that takes place before the saddle-node on a cycle (curve  $l_{sn}(\mu)$  in Fig. 5) in scenario 3. It is through this homoclinic bifurcation that the bursting oscillations arise in the full model. The Poincaré section represents the mapping of some cross section of the flow onto itself. Also indicated is the edge of the 1D stable manifold of the equilibrium point  $E$  which plays a significant role for the behavior of the system.

a saddle which is stable along the manifold  $J_0(\mu)$  with a negative eigenvalue  $\mu^- = -k'\mu + o(\mu) < 0$ . Here,  $|\mu^-|$  is the smaller of  $(|\mu^-|, |-\lambda + o(\mu)|)$ . In this case,  $\mu^-$  defines the leading direction at the 2D stable manifold of  $E$  and, as  $\gamma + o(\mu) > |\mu^-|$ , a saddle cycle is generated from the homoclinic loop under variation of  $l$ . We can therefore postulate that there exists a saddle-node on a cycle bifurcation (+1 multiplier)  $l_{sn}(\mu)$  at which the saddle and stable cycles merge and disappear.

We conclude that the emergence of bursting oscillations cannot be related directly to a homoclinic orbit bifurcation of the fast subsystem. The only way to obtain the transition via a homoclinic orbit of the fast system is to change the parameters  $(l, \mu)$  along the curve  $\mu = \mu_0 |l|^\nu$ ,  $\nu > 1$ . This is a way to a *blue-sky catastrophe* [33, 34].

One may imagine that the saddle-node on a cycle bifurcation  $l = l_{sn}(\mu)$  gives rise to bursting in a straightforward manner. However, we exclude this possibility and state that this saddle-node bifurcation occurs when the saddle-node cycle has a homoclinic orbit. To confirm this, we note that the 2D stable manifold of the saddle cycle has an edge which is the stable 1D manifold  $W^s$  of the equilibrium point  $E$  corresponding to the eigenvalue  $-\lambda + o(\mu)$ . Before the saddle-node bifurcation we meet a homoclinic orbit bifurcation of the saddle cycle which appears when the edge of the stable manifold of this cycle touches its unstable manifold. This occurs when the 1D stable manifold of the equilibrium point  $E$  hits the unstable manifold of the saddle cycle. As illustrated in the Poincaré maps of Figure 6, the homoclinic bifurcation leads to the emergence of a transversal intersection of the stable and unstable manifolds of the saddle cycle. In the present case, a hyperbolic structure in the neighborhood of the homoclinic orbit does not appear but a motion arises along the unstable manifold of the saddle cycle corresponding to bursting. Note that this homoclinic orbit persists under variation of parameter  $l$  up to the value

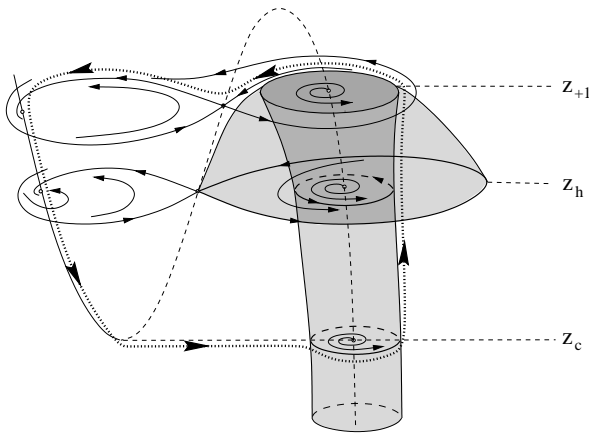


**Fig. 7.** Family of phase portraits for the fast subsystem as a parameter- $z$  bifurcation diagram for scenario 4. The route of bursting oscillations for the full system is illustrated by the dotted curve.

$l_{\text{sn}}(\mu)$ , and the saddle-node on a cycle bifurcation leads to bifurcations of already existing bursting modes.

It is possible that the stable cycle does not reach the saddle-node bifurcation but loses its stability via a multiplier  $-1$  bifurcation (bifurcations via multipliers  $e^{\pm i\varphi}$  are excluded because of the negative divergence of  $\mathcal{F}$  in the vicinity of  $E$ ). In this case the oscillations may become complicated due to period-doubling bifurcations, thus confirming Wang's hypothesis [19]. However this scenario does not affect the bifurcation responsible for the emergence of bursting.

**Scenario 4.** We assume that the conditions corresponding to Figure 7 apply for equation (2.4) and choose the bifurcation parameter  $l = I(z_{+1})$  being the mean value of  $\dot{z}$  along the saddle-node cycle defined by the integral (3.8). In the Hoppensteadt-Izhikevich classification this scenario corresponds to the formation of fold/fold cycle and circle/fold cycle bursters. For  $l < -\varepsilon(\mu) < 0$ , where  $\varepsilon(\mu) \rightarrow 0$ , two cycles exist in the region  $z_h < z < z_{+1}$ , a stable and an unstable one, defined by the roots of the equation  $I(z) = 0$  for  $L_\mu^s$  and  $L_\mu^u$  in accordance with Theorem 4. The stable cycle determines the normal oscillations which represent the steady state of the cell model (2.1).

For  $l > \varepsilon(\mu)$ , the mean value of  $\dot{z}$  at  $U(L_\mu^s)$  is positive, and all trajectories of (2.1) leave  $U(L_\mu^s)$  via  $U(J_2(\mu))$  through the layer  $T_{+1}$  to return to  $U(L_\mu^s)$  via the transitions  $U(J_2(\mu)) \rightarrow U(L_\mu^s)$ . Hence, for  $l > \varepsilon(\mu)$ , bursting oscillations exist and follow the route shown by the dotted curve in Figure 7. It is easy to verify that here we meet the bifurcation of a saddle-node cycle having a homoclinic orbit lying in the transversal intersection of its stable and unstable manifolds. At first sight, this bifurcation looks like the bifurcation in scenario 3 (see Fig. 8(c)). However, as the saddle-node cycle in this case is far away from the equilibrium point  $E$ , the complex limiting set of trajectories that arise, producing chaotic bursting, differs from that of scenario 3.

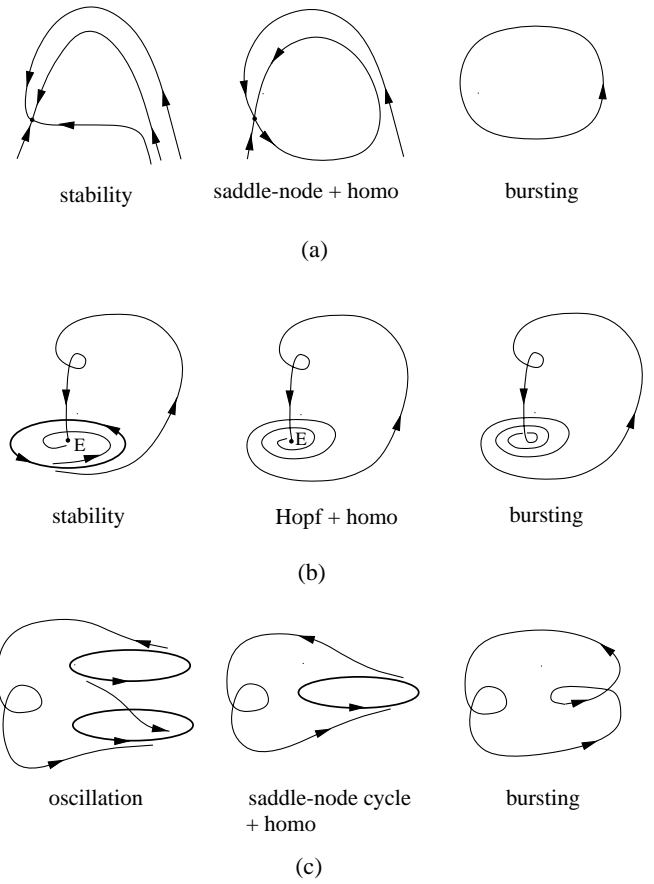


**Fig. 8.** Schematic pictures to illustrate the emergence of bursting oscillations in the various scenarios. (a) Scenario 1: Homoclinic orbit bifurcation of an equilibrium point undergoing a simultaneous saddle-node bifurcation. (b) Scenario 2: Homoclinic orbit bifurcation of a saddle-focus under simultaneous Hopf bifurcation. (c) Scenarios 3 and 4: Homoclinic orbit bifurcations of saddle cycles. In scenario 3, the homoclinic connection passes close to the saddle equilibrium point. In scenario 4, it passes close to a saddle-node cycle for the fast subsystem.

Figure 8 provides a survey of the homoclinic bifurcations involved in the above scenarios. In the first scenario (Fig. 8(a)), the homoclinic bifurcation takes place for an equilibrium point undergoing a simultaneous saddle-node bifurcation. This is a codimension-2 bifurcation with two simultaneously vanishing eigenvalues. In the second scenario, the homoclinic orbit bifurcation occurs for a saddle-focus undergoing a simultaneous Hopf bifurcation. Finally, for scenarios 3 and 4 the homoclinic orbit bifurcation connects the stable and unstable manifolds of a saddle cycle. In scenario 3, the homoclinic connection passes close to the saddle equilibrium point, and in scenario 4 it passes in the vicinity of a saddle-node cycle. In all cases, the formation of a homoclinic connection involves a bifurcation of the full model.

For the case of Figure 7 we may mention another simple bifurcation leading to the emergence of bursting which is related to the location of equilibrium point  $E$  at the right branch of the curve  $z = f(x)$  such that the surface

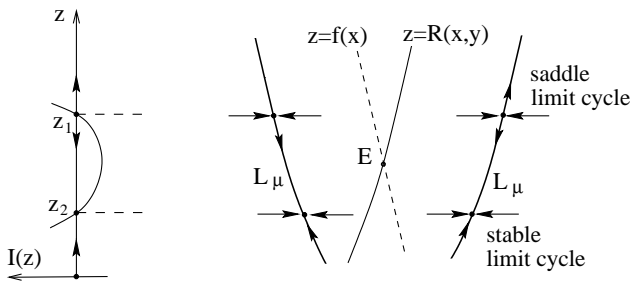


**Fig. 9.** When the integral  $I(z)$  of equation (3.8) vanishes, a stable or unstable limit cycle oscillation may exist in the manifold  $L_\mu$  of scenario 4. The stability of these cycles is determined by  $I'(z)$ , and a stable cycle corresponds to continuous spiking in the cell model. If the cycles disappear, *e.g.*, in a saddle-node bifurcation, bursting oscillations may arise.

$\{z = R(x, y)\}$  intersects the stable manifolds  $L_\mu$  as shown in Figure 9. Applying Theorem 4, we obtain that if the integral  $I(z)$  has a zero  $z_1$ :  $I(z_1) = 0$ ,  $I'(z_1) < 0$ , then the limit cycle  $L_\mu(z_1)$  attracts almost all phase space of system (2.1) and continuous spiking occurs. When, under a shift of the separating surface  $\{z = R(x, y)\}$ , the cycle  $L_\mu(z_1)$  disappears (for example, by merging with a saddle cycle) and  $I(z)$  becomes positive, then bursting arises. Hence we find that the transition from continuous spiking to bursting oscillations takes place via a saddle-node on a cycle “hidden” bifurcation which has no relation to bifurcations of the fast subsystem.

### 5 2D-model map for homoclinic bifurcations

In the above analysis of scenario 3 we have shown how the onset of bursting oscillations can be related to bifurcations within the framework of the following general picture:

A smooth vector field  $\mathcal{F}$  on  $\mathbb{R}^3$  has a unique saddle equilibrium point  $E$  such that the linearized flow at  $E$  has three real eigenvalues, one negative  $-\lambda < 0$  and two positive  $\gamma, \mu > 0$ , satisfying  $\lambda > \gamma \gg \mu > 0$  (here  $-\lambda, \gamma, \mu$  stand for  $-\lambda + o(\mu), \gamma + o(\mu), \mu^+$ ).

Written in the basis of the corresponding eigenvectors, the linearization of  $\mathcal{F}$  is

$$\begin{cases} \dot{x} = -\lambda x, \\ \dot{y} = \gamma y, \\ \dot{z} = \mu z, \end{cases} \quad (5.1)$$

where  $\lambda > 1 \gg \mu > 0$ . For simplicity, we have maintained the old notation for the new variables. At the same time, we have rescaled the time variable  $t \rightarrow \gamma t$ . Hence,  $x$  corresponds to the tangency of the 1D stable manifold  $W^s$  and the plane  $(y, z)$  to the 2D unstable manifold  $W^u$  at  $E$ .

Let us define a disk  $D = \{x = x_0, \|w\| < r\}$  transverse to the flow and intersecting the 1D stable manifold  $W^s$  of the equilibrium point at a distance  $x_0$  from  $E$ . Here,  $\|w\|$  is the norm of the vector  $w = (y, z)$ . As illustrated in Figure 10, we may picture  $D$  as the top disk in a cylindrical half-neighborhood  $U(E)$  with the boundary  $\delta U = D \cup$

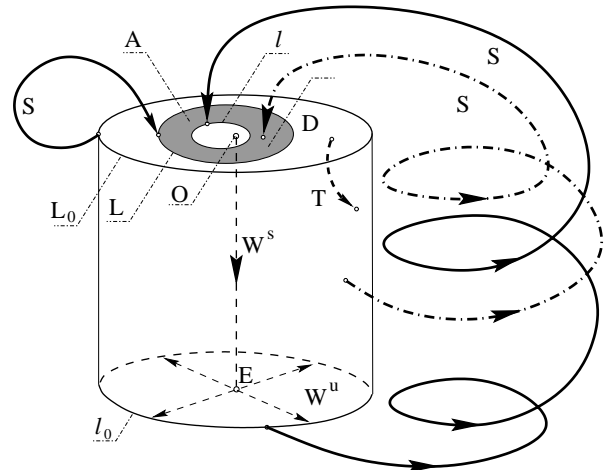


**Fig. 10.** Flow of the vector field around the saddle equilibrium point  $E$  with one negative and two positive eigenvalues. The figure illustrates the construction of a return map of the disk  $D$  into itself. The point  $O$  is mapped via the equilibrium point  $E$  and the curve  $l_0$  into the inner boundary  $l$  of the annulus  $A$ , and the circumference of  $D$  is mapped into the outer boundary  $L$  of  $A$ . For parameters where  $\varphi D \in D$ , the map has an attracting state.

$D_0 \cup d$ . Here,  $d = \{\|w\| = r\}$  denotes the cylindrical side of  $U(E)$ , and  $D_0 = \{W^u \mid \|w\| < r\}$  is a piece of the two-dimensional unstable manifold of  $E$ .

We assume that almost all trajectories starting near  $E$  will return to  $U(E)$  via a transverse intersection of the top disk  $D$ . This assumption is supported by our analyses (Sects. 2 and 3) of the behavior of the trajectories of the cell model for small values of the parameter  $\mu$  defining the ratio of the fast to the slow time constant in equation (2.1) and in a small range of the bifurcation parameter  $l$  near the homoclinic bifurcation in scenario 3. The assumption is also supported by the detailed analyses performed by Terman [20,21]. Exceptions are, of course, trajectories starting from the equilibrium point or from a point on its stable manifold  $W^s$ .

With the above assumption we can conclude that trajectories starting from a point on the cylindrical side  $d$  of  $U(E)$  will return to the top disk  $D$  whatever their particular route in phase space is, either they perform a single fast oscillation or they travel through a slow phase near the silent state and hereafter burst into a series of spikes. Hence, these trajectories define a map  $S : d \rightarrow D$ . In particular, a point on the circumference  $L_0 = \{x = x_0, \|w\| = r\}$  of  $D$  will be mapped into a closed curve  $L = \{x = x_0, \|w\| < r\}$  embedded in  $D$ . The map  $S$  represents the global properties of the system. The form of this map will depend on the precise structure of the cell model as well as on the assumed parameters.

To derive the flow-defined map  $\varphi : D \rightarrow D$  we also need the map  $T : D \rightarrow d$  that describes how trajectories starting in a point of  $D$  are mapped onto the cylindrical surface  $d$ . For the sake of simplicity we assume this map to be determined by the linear flow (5.1) near the equilibrium point. However, this flow has a singularity in  $E$ : The

flow-defined image of the point  $O = W^s \cap D$  for  $t \rightarrow \infty$  is the equilibrium point  $E$ . To remove this singularity we apply the method of extension by continuity. Hence, we represent the image of  $O$  by the closed curve  $l_0 = \{d \cap W^u\}$  that forms the boundary of  $D_0$ , *i.e.*,  $TO = l_0$ .

The equilibrium point  $E$  is the only singular point for the flow. By virtue of the theorem of smooth and continuous variation of the trajectories with their initial conditions [27], the global map  $S$  will be smooth and continuous. After we have removed the singularity in  $E$ , the local map  $T$  is also smooth and continuous. Hence, the combined map  $\varphi = ST$  will be a diffeomorphism. The image  $l = Sl_0$  will be a closed curve embedded in  $D$ . It is also obvious that  $TL_0 = L_0$ . For the Poincaré map  $\varphi = ST$  the images  $l = \varphi l_0$  and  $L = \varphi L_0$  are therefore both closed curves embedded in  $D$ , and we immediately obtain the important result that the image of  $D$  is an annulus  $A = \varphi D$  bounded by the curves  $L$  along the outside and  $l$  along the inside periphery.

In general, the form of the annulus  $A$  will not be circular. By virtue of the complicated global dynamics of the model and the possibility that a trajectory can perform either a single spike or go through a complete bursting phase before it returns to  $D$ , the annulus will be asymmetric and folded. Consider points along some line on the cylinder surface  $d$ . On this line we may locate a particular point starting from where the trajectory completes precisely  $N$  rotations around the right-hand branch of the equilibrium curve for the fast subsystem before it returns to  $D$ . As the initial point gradually moves along the considered line, the rotation of the trajectory in phase space before it returns to  $D$  may increase. As a result, the intersection point with  $D$  will gradually change its angular position. At the same time it also changes its radial position, and as the initial point continues to move along the line, its image in  $D$  produces a spiral. For the whole cylindrical surface, the image will be an annulus that is folded in the form of a spiral. The number of rotations of the spiral and the separation between the spiral arms are controlled by the size of the cylinder and by the parameter  $\mu$ . The rotations of the trajectory around the right-hand branch of the equilibrium curve has a finite amplitude, and each rotation takes a finite time. For a finite (*i.e.* non-vanishing) value of  $\mu$ , the vertical shift of the trajectory per rotation will also be finite. Hence, it is possible to define the size and shape of the cylinder such that neighboring points with different number of rotations of the trajectory do not arise. This is precisely the problem that Terman emphasizes [20,21]. However, in view of the fact that the type of homoclinic bifurcation that we are facing does not appear to have been previously analyzed in detail, we have decided in the following analysis to neglect the complexity associated with the rotations of the trajectory during the bursting phase and assume the simplest possible version of the global map  $S$ . As previously noted, our goal is to show that the combined map  $\varphi$  can produce stable chaotic bursting.

Let us pause for a moment to consider the unusual properties of the Poincaré map  $\varphi : D \rightarrow D$ . An essen-

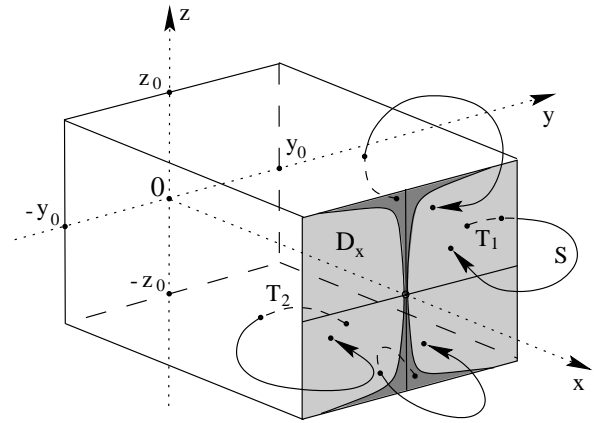


**Fig. 11.** Cross-sections for constructing the model map along the trajectories of (5.1) in a small neighborhood of  $E$ . The coordinate system has been shifted so that  $(0, 0, 0)$  represents the saddle equilibrium point  $E$  and the directions  $x, y$ , and  $z$  are the eigendirections at this point.  $x$  is the contracting direction, and  $y$  and  $z$  are the directions with positive eigenvalues. The return map is obtained as a composition of the local map  $T : D \rightarrow d$  and the global map  $S : d \rightarrow D$ .

tial aspect of this map is that it generates an annulus  $A$  with a hole  $H_0$  whose external boundary  $l$  is the image of the point  $O$  through the doubly unstable equilibrium point  $E$ . The composition of this saddle point, that part of its unstable manifold  $W^u$  that connects it to  $l$ , and the hole  $H_0$  defines a heart-formed trapping zone  $\Omega$ . This zone has the property that all trajectories starting within  $\Omega$  will remain there for ever. Trajectories from the outside can enter  $\Omega$  through the hole  $H_0$ . For  $O \subset A$ , the image of  $A$  is an annulus surrounding  $H_0$  and having a new hole  $\varphi H_0 \subset \varphi A$ . For a sufficiently small neighborhood  $U(O)$ ,  $\varphi U(O) \cap \varphi H_0 = O$ , and  $\varphi U(O) \subset \varphi A$ . Under these conditions, the repeated image  $\varphi^k A$  is an “annulus” with  $k + 1$  holes.

As the parameters of the cell model are changed, the position of the annulus  $A$  relative to the point  $O$  will also change. In particular when  $O$  passes the curve  $l$  moving from the hole  $H_0$  into the annulus  $A$  a homoclinic cycle is generated as a fixed point for  $\varphi$  lying in  $A$ . In order to understand the role of this bifurcation for the global behavior of the system let us note that:

- i) for  $O \in H_0$  (as illustrated in Fig. 10), the image  $\varphi A$  is an annulus lying in  $A$  and surrounding the hole  $H_0 \cup \varphi U(O)$ , and
- ii) for  $O \in l$  when the system attains a homoclinic orbit of the saddle  $E$ , the annulus  $\varphi U(O)$  is composed of two parts: One part lies in  $\varphi A$  and the other part lies in  $\varphi H_0$ .

To construct a simplified version of our 2D map let us consider the problem in a rectangular coordinate system. As illustrated in Figure 11,  $U(E) = \{0 \leq x \leq x_0, |y| \leq y_0, |z| \leq z_0\}$  is a half-neighborhood of the saddle  $E$ . We denote the cross-section disk  $D_x = \{x = x_0, |y| \leq y_0, |z| \leq z_0\}$  and the lateral area of  $U(E)$ ,  $d = d_1 \cup d_2 \cup \bar{d}_1 \cup \bar{d}_2$ , where  $d_{1,2} = \{y = \pm y_0, 0 < x < x_0, |z| < z_0\}$  and  $\bar{d}_{1,2} =$

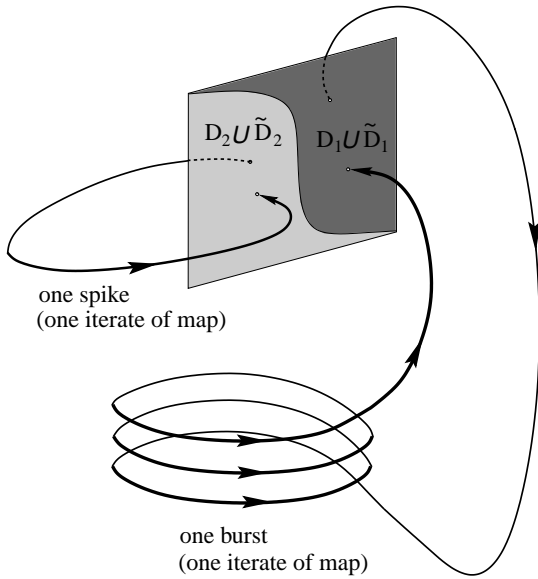


**Fig. 12.** Action of the map  $\varphi$  on the rectangle (topological disk)  $D_x = \{D_1 \cup \tilde{D}_1 \cup D_2 \cup \tilde{D}_2\}$ . The iterate  $\varphi M$  of a point  $M \in D_1 \cup \tilde{D}_1$  assimilates one turn along the route of the left branch  $J_1(\mu)$  and the manifold  $L_\mu$ , representing one burst of oscillations. The iterate  $\varphi M$  of a point  $M \in D_2 \cup \tilde{D}_2$  represents one turn near the homoclinic loop of the fast subsystem (*i.e.*, one spike). Chaotic dynamics may be realized through mapping of points from one region into the other.

$\{z = \pm z_0, 0 < x < x_0, |y| < y_0\}$ . The point  $O = \{x = x_0, y = z = 0\}$  and its image  $l_0 = l_{01} \cup l_{02} \cup \tilde{l}_{01} \cup \tilde{l}_{02}$ , where  $l_{01,2} = \{x = 0, y = \pm y_0, |z| < z_0\}$ ,  $\tilde{l}_{01,2} = \{x = 0, z = \pm z_0, |y| < y_0\}$ .

The local map  $T : D_x \rightarrow d$  may be constructed via the obvious solutions of (5.1)  $x(t) = x_{(0)}e^{-\lambda t}$ ,  $y(t) = y_{(0)}e^t$ ,  $z(t) = z_{(0)}e^{\mu t}$ . For small  $U(E)$  this map is generic, because (5.1) is the appropriate normal form. Our assumption that the manifold  $W^u$  returns to  $D_x$  implies the existence of the global map  $S : d \rightarrow D_x$  with  $S$  being some diffeomorphism defined by (2.1).

Let us use the rescaled variables  $(x/x_0, y/y_0, z/z_0)$  with the passage times  $\tau = -\ln y$  for the map  $T_{1,2} : D_x \rightarrow d_{1,2}$  and  $\tilde{\tau} = -(1/\mu)\ln y$  for the map  $\tilde{T}_{1,2} : D_x \rightarrow \tilde{d}_{1,2}$  (in rescaled  $y$  and  $z$ ). In terms of the new variables,  $D_x = \{x = 1, |y| \leq 1, |z| \leq 1\}$ ,  $d_{1,2} = \{y = \pm 1, 0 \leq x(\tau) \leq 1, |z(\tau)| \leq 1\}$ , and  $\tilde{d}_{1,2} = \{z = \pm 1, 0 \leq x(\tilde{\tau}) \leq 1, |y(\tilde{\tau})| \leq 1\}$ .

Then the map  $T$  may be written in the form

$$\begin{aligned} T_{1,2} : \quad & x(\tau) = |y|^\lambda, \quad \text{for } |z| \leq |y|^\mu; \\ & z(\tau) = |y|^{-\mu} z, \\ \tilde{T}_{1,2} : \quad & x(\tilde{\tau}) = |z|^{\lambda/\mu}, \quad \text{for } |z| \geq |y|^\mu; \\ & y(\tilde{\tau}) = |z|^{-1/\mu} y. \end{aligned} \quad (5.2)$$

We denote the regions of the disk  $D_x$ , where the map  $T$  has different actions as  $D_{1(2)} = \{|z| \leq |y|^\mu, y > 0 (y < 0)\}$  and  $\tilde{D}_{1(2)} = \{|z| \geq |y|^\mu, z > 0 (z < 0)\}$  (see shaded regions in Fig. 11). The successive flow-defined global map

$S$ , also separated into four parts and smoothly joining with  $T$  at  $|z| = |y|^\mu$ , produces the resulting return map  $\varphi = ST : D_x \rightarrow D_x$ .

To relate the map  $\varphi$  to the behavior of the cell model (2.1), as illustrated in Figure 12 we assume that the iterate  $\varphi M$  of a point  $M \in D_2 \cup \tilde{D}_2$  simulates one turn near to the homoclinic loop of the fast system (one spike), and that the iterate  $\varphi M$  of a point  $M \in D_1 \cup \tilde{D}_1$  simulates one turn along the route of the left branch  $J_1(\mu)$  and manifold  $L_\mu$  representing one burst of oscillations. Hence, any attractor of the map  $\varphi^{(s)} = ST_2(ST_2)$  is related to continuous spiking and any attractor of any composition of  $\varphi^{(s)}$  and  $\varphi^{(b)} = ST_1(ST_1)$  to burstings. This may be seen as a formalization of Wang's discussion [19] of a symbolic dynamics approach to characterize different modes of alternating spikes and bursts.

## 6 Symmetric model map

To obtain an explicit form of the map  $\varphi$  we replace  $|y|^\mu$  in (5.2) by its  $\mu \rightarrow 0$  limit of 1, thus avoiding the construction of  $S\tilde{T}$  and eliminating the dark grey regions  $\tilde{D}_{1,2}$  of Figure 11. With this approximation the image  $\varphi D_x$  becomes two separate pieces of the annulus, and the map  $\varphi$  becomes discontinuous. Furthermore, for the sake of simplicity we assume the map to have the central symmetry  $\varphi(-y, -z) = -\varphi(-y, -z)$  and consider only constant and linear contributions to the maps  $S_{1,2} : d_{1,2} \rightarrow D_x$ ,

$$\begin{pmatrix} \bar{y} \\ \bar{z} \end{pmatrix} = S_1 \begin{pmatrix} x(\tau) \\ z(\tau) \end{pmatrix} = A \begin{pmatrix} x \\ y \end{pmatrix} + \begin{pmatrix} -\alpha \\ \gamma \end{pmatrix}, \quad y > 0, \quad (6.1)$$

where  $A = \|a_{i,j}\|$ ,  $i, j = 1, 2$  is a nonsingular  $2 \times 2$  matrix.  $\alpha$  and  $\gamma$  are bifurcation parameters. With these approximations, the map  $\varphi$  reduces to

$$\begin{cases} \bar{y} = (-\alpha + a_{11}|y|^\lambda \operatorname{sgn} y + a_{12}z), \\ \bar{z} = (\gamma + a_{21}|y|^\lambda) \operatorname{sgn} y + a_{22}z. \end{cases} \quad (6.2)$$

Let us further restrain the analysis to non-twisted maps  $S_{1,2}$ , assuming that  $a_{12} \equiv -\delta \leq 0$ , and  $a_{11}, a_{12}, a_{22} > 0$ . For simplicity we also take  $\gamma \geq 0$ . A complete analysis of the full map will be presented in a separate publication.

The map  $\varphi$  is discontinuous at  $y = 0$ , and as shown in Figure 13 the images  $\varphi_1 D_1$  and  $\varphi_2 D_2$  are symmetric parallelograms such that the segments  $N_1 N_2$  and  $\bar{N}_1 \bar{N}_2$  are related to the images of the stable manifold  $W^s : \varphi_1(0, 0) = N_1 N_2$ ,  $\varphi_2(0, 0) = \bar{N}_1 \bar{N}_2$ , thus identifying the segments ( $y = 0, |z| < c$ ) with the origin  $(0, 0)$  in accordance with the substitution  $|y|^{-\mu} z \cong z$ .

The condition  $\varphi D_x \subset D_x$  for (6.2) takes the form

$$\begin{aligned} 1 - \delta > \alpha > 1 + a_{11} + \delta, \\ -1 + a_{22} < \gamma < 1 - a_{22} - a_{21}. \end{aligned} \quad (6.3)$$

A *homoclinic orbit* exists when  $(0, 0) \in N_1 N_2 ((0, 0) \in \bar{N}_1 \bar{N}_2)$ . This condition gives the bifurcation line

$$\alpha = \alpha^{(h)} \equiv \frac{\delta}{a_{22}} \gamma, \quad |\gamma| \leq a_{22}. \quad (6.4)$$

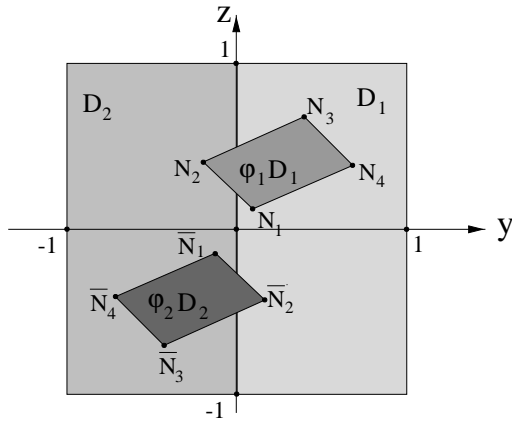


**Fig. 13.** The parallelograms  $\varphi_1 D_1$  and  $\varphi_2 D_2$  arise as the first images of the regions  $D_1$  and  $D_2$  under the action of the symmetric map. This map is obtained in the limit  $\mu \rightarrow 0$  where  $\mu$  represents the smallest of the two positive eigenvalues for the saddle point  $E$ . The line segments  $N_1 N_2$  and  $\bar{N}_1 \bar{N}_2$  are images of the origin, and a homoclinic orbit exists when  $(0, 0) \in N_1 N_2$  (or  $(0, 0) \in \bar{N}_1 \bar{N}_2$ ).

Fixed points of the map  $\varphi$  are defined by the equations  $\bar{y} = y > 0$ , and  $\bar{z} = z$ . From (6.2) we obtain

$$\begin{cases} z_1(y) = \delta^{-1}(-\alpha + a_{11}y^\lambda - y), \\ z_2(y) = (1 - a_{22})^{-1}(\gamma + a_{21}y^\lambda), \end{cases} \quad (6.5)$$

such that the equation  $g_1(y) \equiv z_1(y) - z_2(y) = 0$  defines the coordinates  $y$  of the fixed points. It is obvious that the map  $\varphi_1(\varphi_2)$  has the stable fixed point  $p_1(y_1, z_1(y_1))(p_2)$  and the saddle point  $p_1^*(y_1^*, z_1(y_1^*))(p_2^*)$ ,  $0 < y_1 < y_1^*$ ,  $y_2^* < y_2 < 0$ , respectively), for some interval

$$\alpha^{(1)} - A_1 < \alpha < \alpha^{(1)}. \quad (6.6)$$

The bifurcation value

$$\alpha = \alpha^{(1)} \equiv -\frac{\delta\gamma}{1 - a_{22}} \quad (6.7)$$

corresponds to the disappearance of  $p_1$  and  $p_2$  at the edge of  $D_{1,2}$  ( $y = 0$ ), and the value  $\alpha^{(1)} - A_1$  is the saddle-node bifurcation of  $p_1$  and  $p_1^*$ . Being a solution to the system  $g_1 = 0$ ,  $(g_1)'_y = 0$  with respect to  $\alpha$ , this gives

$$A_1 = \lambda^{-(\lambda/(\lambda-1))} (1 + \lambda) \left( \frac{1 - a_{22}}{a_{11} - \Delta} \right)^{1/(\lambda-1)}. \quad (6.8)$$

The symmetric period-2 cycles is defined by the condition  $\{\bar{y} = -y < 0, \bar{z} = -z\}$ . Arising from (6.2), the equation

$$g_2(y) \equiv (\delta(1 + a_{22}))^{-1} \times (\alpha_0 + (1 + a_{22})y + (a_{11} + \Delta)y^\lambda) = 0, \quad (6.9)$$

where  $\alpha_0 = -\alpha(1 + a_{22}) + \gamma\delta$ ,  $\Delta = \det A > 0$  then determines the  $y$ -coordinates of the period-2 symmetric cycle.

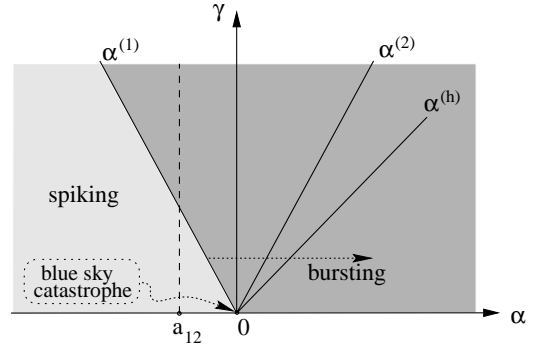


**Fig. 14.** Schematic phase diagram for the map (6.1). The light grey zone represents the region of continuous spiking. Transitions across  $\alpha^{(1)}$  lead to bursting.  $\alpha^{(1)}$  represents the disappearance of a stable, respectively, an unstable cycle at the edge of  $D_{1,z}$  and the appearance of a period-2 cycle.  $\alpha^{(2)}$  is a pitchfork bifurcation where the period-2 cycle is replaced by two different cycles of the same period.  $\alpha^{(h)}$  is a line of homoclinic bifurcations. Transitions through the origin  $(\alpha, \gamma) = (0, 0)$  correspond to a blue sky catastrophe. (Due to the symmetry of the map, the transition from spiking to bursting takes place via a heteroclinic bifurcation that occurs close to  $\alpha^{(1)}$ ).

For  $\alpha_0 > 0$ , equation (6.9) has no solutions. For  $\alpha_0 < 0$ , a unique solution of (6.9) corresponding to the symmetric period-2 cycle  $C_2((y^*, z^*) : (-y^*, -z^*) = f(y^*, z^*))$  is generated from the boundary  $\{y = 0\}$  at the bifurcation line ( $\alpha_0 = 0$ ):

$$\alpha = \alpha^{(2)} \equiv \frac{\delta\gamma}{1 + a_{22}}. \quad (6.10)$$

This cycle is stable in the interval

$$\alpha^{(2)} < \alpha < \alpha^{(2)} + A_2, \quad (6.11)$$

where

$$A_2 = \left( \frac{1 - a_{22}}{\lambda(a_{11} - \Delta)} \right)^{1/(\lambda-1)} \times \left( 1 + \frac{(a_{11} + \Delta)(1 - a_{22})}{\lambda(a_{11} - \Delta)(1 + a_{22})} \right). \quad (6.12)$$

At the bifurcation value  $\alpha^{(2)} + A_2$  the cycle  $C_2$  becomes unstable, and two stable asymmetric period-2 cycles  $C_2^+$  and  $C_2^-$  are generated from  $C_2$ .

The arrangement of the bifurcation lines (6.4), (6.7), (6.10) and the domains (6.6), (6.11) are illustrated in Figure 14. Obviously, from the previous local analysis we may conclude that for  $\alpha > \alpha^{(2)}$ , bursting oscillations exist. In order to obtain the general picture of the emergence of the bursting oscillations let us consider the nonlocal behavior of the map  $\varphi$  in the region of parameters  $\alpha < \alpha^{(2)}$ .

**Theorem 5.** Let the conditions (6.3) and

$$\lambda(-\alpha + \alpha_{11})^{\lambda-1} < \frac{1 - a_{22}}{a_{11} - \Delta} \quad (6.13)$$

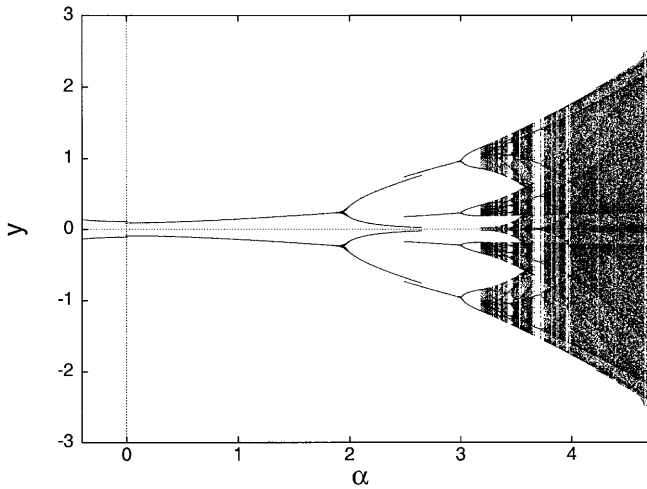


**Fig. 15.** Bifurcation diagram for the symmetric model map (6.2) with  $\alpha$  as the active parameter. The other parameters are  $a_{11} = 0.4, a_{12} = -0.1, a_{21} = a_{22} = \gamma = 0.1$ , and  $\lambda = 2$ . The transition to chaos does not occur via period-doubling but via an unusual cascade of pitchfork and boundary collision bifurcations.

be satisfied. Then

- 1) for  $\alpha \leq -\delta$  the fixed points  $p_1$  and  $p_2$  are globally stable so that  $D_1(D_2)$  is the basin of  $p_1$  ( $p_2$ , respectively);
- 2) for  $\alpha^{(1)} > \alpha > -\delta$  the basin of each stable point  $p_1$  and  $p_2$  consists of parts of  $D_1$  and  $D_2$ ;
- 3) for  $\alpha > \alpha^{(1)}$  the map  $\varphi$  has the limiting set of composition  $\varphi_2 \circ \varphi_1$ .

**Proof.** 1) Due to (6.3),  $\varphi_{1,2}D_1 \subset D_{1,2}$  for  $\alpha \leq -\delta$  and since (6.3) implies the contraction of  $\varphi$  at  $\varphi D_x$ , the points  $p_1$  and  $p_2$  are globally stable in  $D_1$  and  $D_2$ , respectively.

2) For  $\alpha^{(1)} > \alpha > -\delta$ ,  $p_1 \in \varphi_1 D_1$  and  $p_2 \in \varphi_2 D_2$ , but as  $q_2 = \varphi_1 D_1 \cap D_2 \neq \emptyset$  ( $q_1 = \varphi_2 D_2 \cap D_1 \neq \emptyset$ ) the basins of  $p_1$  and  $p_2$  consist of parts of  $D_1$  and  $D_2$ .

3) For  $\alpha = \alpha^{(1)}$ ,  $p_1$  and  $p_2$  lie at the boundary  $\{y = 0\}$ , and the domains  $q_1$  and  $q_2$  adjoin the fixed points  $p_1$  and  $p_2$ . Moreover,  $\varphi_2^n q_2 \rightarrow p_2$ ,  $\varphi_1^n q_1 \rightarrow p_1$  for  $n \rightarrow \infty$ . Hence, there exists a heteroclinic linkage of  $p_1$  and  $p_2$  so that the composition  $\varphi_2 \circ \varphi_1$  for  $\alpha > \alpha^{(1)}$  has the limiting set generated from this linkage.  $\square$

Now we have the following explanation of the onset of bursting oscillations through the symmetric model map (6.2). For  $\gamma = \text{const} \geq 0$ ,  $\delta \neq 0$ , while  $\alpha$  is increasing the birth of a limiting set for the composed map  $\varphi_2 \circ \varphi_1$  (bursting oscillations) occurs at  $\alpha = \alpha^{(1)}$  via the creation of a heteroclinic linkage of the stable points  $p_{1,2}$  situated at the boundary of the map discontinuity. For our initial continuous system, the bifurcation of  $p_{1,2}$  at the boundary  $\{y = 0\}$  corresponds to a saddle-node bifurcation. One can easily verify this fact by using the map (6.2) with return term  $y^{-\mu}z$  instead of  $z$ . Thus we obtain that the establishment of a heteroclinic linkage between the points  $p_1$  and  $p_2$  represents the bifurcation in which the 1D stable manifold of  $E$  hits the unstable manifold of the

saddle cycle. This corresponds to the situation in Figure 6. The blue sky catastrophe discussed in Section 4 is modeled by the map (6.2) when  $\alpha, \gamma \rightarrow 0$  along the ‘‘tongue’’  $0 < \gamma < -(1 - a_{22})\alpha/\delta$ , *i.e.*, through a codimension-2 homoclinic bifurcation.

The bifurcation diagram for the symmetric map is illustrated in Figure 15 for particular values of the parameters. Observe that the increase of  $\alpha$  leads to chaos. At first sight the diagram may appear similar to that of a period-doubling scenario. However, the present scenario is quite different. The change of the periods occurs only through gaps when periodic orbits reach the boundary  $\{y = 0\}$ . The pitchfork-like branches correspond to loss of stability of symmetric orbits (one multiplier becomes equal to +1) while two asymmetric orbits with the same period appear.

For negative values of  $\alpha$  ( $\alpha < \alpha^{(1)} \cong -0.01$ ), the map (6.2) exhibits two stable fixed points. One of these corresponds to continuous spiking (repeated application of  $\varphi_2$ , see, *e.g.*, Fig. 12). The other fixed point exists due to the symmetry of the map and has no real significance. For positive values of  $\alpha$  ( $0.01 \cong \alpha^{(2)} < \alpha < \alpha^{(2)} + A_2 \cong 1.96$ ) the map exhibits a period-2 orbit corresponding to a regular alternation of bursts and spikes (one iteration of  $\varphi_1$  followed by one iteration of  $\varphi_2$ , etc.). At  $\alpha = \alpha^{(2)} + A_2$ , the period-2 orbit undergoes a pitchfork bifurcation, and for  $\alpha^{(2)} + A_2 < \alpha < \alpha_4^{(1)} \cong 2.5$ , two asymmetric period-2 orbits coexist. At  $\alpha = \alpha_4^{(1)}$ , a period-4 orbit arises in a saddle-node bifurcation (multiplier +1), and at  $\alpha = \alpha_4^{(2)} \cong 2.7$ , the two period-2 orbits disappear in a boundary collision bifurcation. For  $\alpha \cong 3.0$ , the period-4 orbit undergoes a pitchfork bifurcation and produces two mutually symmetric period-4 cycles. As follows from this description, the transition from continuous spiking to bursting takes place in a small interval around  $\alpha = 0$ . Due to the symmetry of the map, this transition does not take place via a homoclinic bifurcation, but via the creation of a heteroclinic connection. This aspect of the map (6.2) disappears when we introduce asymmetries.

## 7 Asymmetric model map

Consider again the model map  $\varphi = ST$ . For scenario 3 the flow system (2.1) must be asymmetric. While maintaining simplicity we may take this asymmetry into account by changing only a single parameter  $\alpha$  for  $y < 0$ :

$$\begin{cases} \bar{y} = -\alpha + a_{11}y^\lambda - \delta z, & y \geq 0, \\ \bar{y} = \beta - a_{11}|y|^\lambda - \delta z, & y < 0, \\ \bar{z} = (\gamma + a_{11}|y|^\lambda) \text{sgn } y + a_{22}z. \end{cases} \quad (7.1)$$

Assume  $\beta = \text{const} > 0$ , so that  $\varphi_2$  has no stable fixed points and the region  $D_2$  becomes transient under  $\varphi_2$ , and consider the bifurcations of (7.1) that occur when changing the parameter  $\alpha$ .

- 1) For  $\alpha = \alpha^{(1)}$  the fixed point  $p_1$  of  $\varphi_1$  is globally stable. At the boundary bifurcation when  $p_1 \in \{y = 0\}$ , homoclinic orbits of  $p_1$  exist, and the transition to  $\alpha > \alpha^{(1)}$

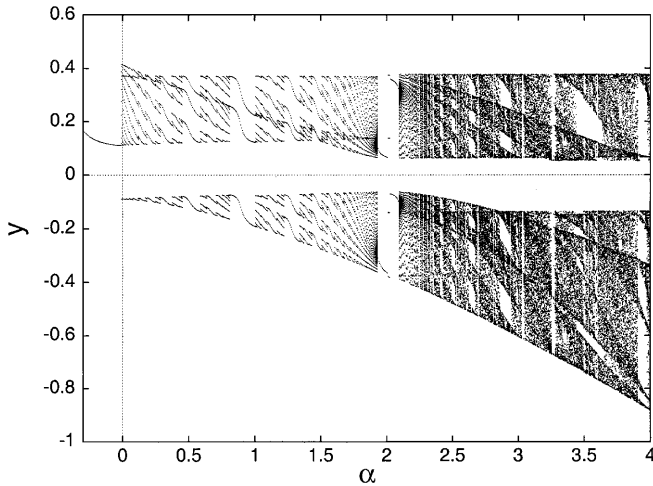


**Fig. 16.** Bifurcation diagram for the asymmetric model map (7.1). The parameters are  $a_{11} = \beta = 1$ ,  $\delta = \gamma = a_{22} = 0.1$ , and  $\lambda = 1.5$ . In this case the map only shows a single fixed point corresponding to continuous spiking for negative values of  $\alpha$ .

corresponds to the birth of a limiting set of the two-sided map  $\varphi$ . For scenario 3 this bifurcation may be interpreted as follows. When the stable cycle of the cell model (2.1) passes into the layer  $T_h$ , it merges with the saddle-type cycle born from the homoclinic orbit of the saddle equilibrium point ( $p_1$  reaches  $y = 0$ ). Before the bifurcation point, the saddle cycle  $C^{\text{sd}}$  has a homoclinic orbit following the route  $C^{\text{sd}} \rightarrow U(J_1(\mu)) \rightarrow T_1 \rightarrow U(L_\mu^s) \rightarrow C^{\text{sd}}$ . The appearance of this homoclinic orbit leads to the bursting oscillations. The blue sky catastrophe occurs, similarly to the symmetric case when  $\alpha, \gamma \rightarrow 0$  along the tongue  $0 < \gamma < -(1 - a_{22})\alpha/\delta$  such that the point  $p_1$  reaches zero, *i.e.*, the stable limit cycle merges with the homoclinic orbit of the equilibrium point.

Figure 16 displays the bifurcation diagram for the asymmetric map (7.1). The gaps in the diagram arise from destroyed pitchfork-like branches because of lack of symmetry. Complex bursting oscillations may arise before the bifurcation of the saddle-node cycle having a homoclinic orbit. This explosive transition from a fixed point to complex solutions is clearly seen in Figure 16. Finally, we observe that for  $\delta = 0$ , the map  $\varphi$  attains a triangular form, and we find the simple 1D non-invertible map for  $\varphi$ :

$$\begin{cases} \bar{y} = -\alpha + ay^\lambda, & y \geq 0, \\ \bar{y} = \beta - b|y|^\lambda, & y < 0. \end{cases} \quad (7.2)$$

Being independent of the coordinate- $z$  part of the invertible map (6.2) (or (7.1)), this new map maintains all the main features (with the simplification that  $\alpha^{(1)} = \alpha^{(2)} = \alpha^{(h)} = 0$ ). Hence, it may be considered as a basic factor-map for our model.

## 8 Conclusions and remarks

The main conclusion of this paper is as follows. Phase portraits of the fast subsystem (Figs. 3, 4, 7 and other

possible versions) are well known. In the same way, “on-off” mechanisms for bursting are trivially understood in the case of a suitable location of the slow equation surface  $\{R(x, y) - z = 0\}$  separating the left and right branch attractors. However, the mechanism of the onset of bursting under a shift of the function  $R(x, y)$  is “hidden” and may be clarified only through a detailed study of the bifurcations of nontrivial homoclinic orbits that do not exist in the fast system.

The details of the bifurcations for scenarios 2 and 4, especially the construction of matching, explicitly defined maps will be the subject of a separate study. As for scenario 3, the next step is a construction of the full modeling map of the disk into an annulus including an investigation of the general nonlocal map defined by the nontrivial topological structure of the manifolds of Figure 10.

The specific form of the model map considered in Sections 6, 7 came from our simplifying assumptions combined with the approximation of an obviously strongly nonlinear map  $S$  by a linear one. Even in this case we obtained a good accordance of the bursting chaotic oscillations with the behavior predicted by our qualitative analysis. For the purpose of simplicity we eliminated the domains  $\tilde{D}_{1,2}$  with the loss of continuity and the transformation of the annulus into two separated domains as results. What would happen if  $\tilde{D}_{1,2}$  were reintroduced, and the map  $S$  considered in its full nonlinear form? We may present the following preliminary answer to this question. First, in this case the image  $\varphi D_x$  becomes the annulus  $A$  and the image  $\varphi \tilde{D}_1 \subset A$ . We assume that the map  $S$ , depending of some parameter  $r$ , acts as a returning nonlinear twist map such that parts of  $A$  that are farther from zero rotate faster than nearer parts and this rotation increases with the parameter  $r$ . Then for some value  $r_0$  a tangency of  $\tilde{D}_1$  and  $\varphi \tilde{D}_1$  occurs and this will signal the beginning of the formation of a Smale horseshoe. For  $r_1 > r_0$ ,  $\varphi \tilde{D}_1$  intersects  $\tilde{D}_1$  transversely, for  $r_2 > r_1$  a new intersection occurs, and so forth. Then the interval  $(r_0, r_1)$  will have a Newhouse set [35], the values  $r_1, r_2, \dots$  being the winding numbers of Terman corresponding to the increase of kneading of the hyperbolic set.

We would like to thank L.P. Shil’nikov for his continuous interest in the present study and many helpful discussions. VB and IB acknowledge support from the Danish Research Academy. This work was also supported in part by RFFI (grant No. 99-01-01126) and by grant “Universities of Russia” (No. 1905).

## References

1. A.J. Vander, J.H. Sherman, D.S. Luciano, *Human Physiology: The Mechanisms of Body Function* (McGraw Hill, New York, 1980).
2. A.L. Hodgkin, A.F. Huxley, *J. Physiol.* **117**, 500 (1952).
3. L.L.Constantin, in: *Handbook of Physiology*, Sect. I: *The Nervous System*, edited by V.B. Mountcastle, J.M. Brookhart (American Physiological Society, Bethesda, 1977).

4. E. Bülbring, A.F. Brading, A.W. Jones, T. Tomita, *Smooth Muscle* (Edward Arnold, London, 1970).
5. W.B. Adams, J.A. Benson, *Prog. Biophys. Molec. Biol.* **46**, 1 (1985).
6. I. Atwater, B. Riballet, E. Rojas, *J. Physiol.* **278**, 117 (1978).
7. A. Sherman, P. Carroll, R.M. Santos, I. Atwater, in: *Transduction in Biological Systems*, edited by C. Hidalgo, J. Bacigalupo, E. Jaimovich, J. Vergara (Plenum, New York, 1990).
8. L. Satin, D. Cook, *Eur. J. Physiol. (Pflügers Arch.)* **414**, 1 (1989).
9. R.E. Plant, M. Kim, *Biophys. J.* **16**, 227 (1976).
10. C. Morris, H. Lecar, *Biophys. J.* **35**, 193 (1981).
11. T.R. Chay, J. Keizer, *Biophys. J.* **42**, 181 (1983).
12. J. Rinzel, Y.S. Lee, in: *Nonlinear Oscillations in Biology and Chemistry, Lecture Notes in Biomathematics*, Vol. **66**, edited by H.G. Othmer (Springer-Verlag, New York, 1986).
13. D.M. Himmel, T.R. Chay, *Biophys. J.* **51**, 89 (1987).
14. M. Colding-Joergensen, H. Ostergaard Madsen, B. Bodholdt, E. Mosekilde, *J. Theor. Biol.* **156**, 309 (1992).
15. P. Smolen, J. Keizer, *J. Membrane Biol.* **127**, 9 (1992).
16. M.R. Guevara, T.J. Lewis, *Chaos* **5**, 174 (1995).
17. P. Smolen, J. Rinzel, A. Sherman, *Biophys. J.* **64**, 1668 (1993).
18. J.L. Hindmarsh, R.M. Rose, *Proc. Roy. Soc. London Ser. B* **221**, 87 (1984).
19. X.-J. Wang, *Physica D* **62**, 263 (1993).
20. D. Terman, *J. Nonlinear Sci.* **2**, 135 (1992).
21. D. Terman, *SIAM J. Appl. Math.* **51**, 1418 (1991).
22. T.R. Chay, *Physica D* **16**, 233 (1985).
23. Y.S. Fan, T.R. Chay, *Biol. Cybern.* **71**, 417 (1994).
24. F.C. Hoppensteadt, E.M. Izhikevich, (Springer-Verlag, New York, 1997).
25. V.N. Belykh, *Differential Equations* **11**, 2083 (1975).
26. L.N. Belyustina, V.N. Belykh, *Izv. Vuzov, Radiofizika* **15**, 1039 (1972).
27. V.I. Arnold, V.S. Afraimovich, Y.S. Iljashenko, L.P. Shil'nikov, *Dynamical Systems Bifurcation Theory and Catastrophe Theory*, Vol. **5** (Springer-Verlag, New York, Berlin, Heidelberg, 1994).
28. L.S. Pontrjagin, *Phys. Zeit. Sowjetunion* **6**, 1 (1934).
29. E.M. Izhikevich, *Subcritical elliptic bursting*, preprint.
30. L.A. Belyakov, *Math. Zametki* **36**, 838 (1984).
31. V.N. Belykh, Yu.S. Chertkov, *Boundary Value Problems, Mezhvuz. Sbornik, Perm' Politech. Inst. Perm'*, 120 (1980).
32. L.P. Shil'nikov, *Math. USSR Sbor.* **6**, 427 (1968).
33. J. Palis, C. Pugh, *Lect. Notes Math.* **468**, 345 (1975).
34. D.V. Turaev, L.P. Shil'nikov, *Dokl. Akad. Nauk* **342**, 596 (1995).
35. S.E. Newhouse, *Publ. Math. IHES* **50**, 101 (1979).